

CHEMISTRY

A European Journal

A Journal of



Accepted Article

Title: Dendritic and Core-Shell-Corona Mesoporous Sinter Nanospheres from Polymer-Surfactant-Silica Self-Entanglement

Authors: Kun Zhang

This manuscript has been accepted after peer review and appears as an Accepted Article online prior to editing, proofing, and formal publication of the final Version of Record (VoR). This work is currently citable by using the Digital Object Identifier (DOI) given below. The VoR will be published online in Early View as soon as possible and may be different to this Accepted Article as a result of editing. Readers should obtain the VoR from the journal website shown below when it is published to ensure accuracy of information. The authors are responsible for the content of this Accepted Article.

To be cited as: *Chem. Eur. J.* 10.1002/chem.201704714

Link to VoR: <http://dx.doi.org/10.1002/chem.201704714>

Supported by
ACES

WILEY-VCH

DOI: 10.1002/ ((please add manuscript number))

Article type: Full Paper

Dendritic and Core-Shell-Corona Mesoporous Sister Nanospheres from Polymer-Surfactant-Silica Self-Entanglement

Kun Zhang, Tai-Qun Yang, Bing-Qian Shan, Peng-Cheng Liu, Bo Peng, Qing-Song Xue, En-Hui Yuan, Peng Wu,* el én Albela, Laurent Bonneviot**

Prof. Kun Zhang, Tai-Qun Yang, Bing-Qian Shan, Peng-Cheng Liu, Bo Peng, Dr. Qing-Song Xue, En-Hui Yuan, Prof. Peng Wu
Shanghai Key Laboratory of Green Chemistry and Chemical Processes, School of Chemistry and Molecular Engineering
East China Normal University
Shanghai, 200062, China
E-mail: kzhang@chem.ecnu.edu.cn, pwu@chem.ecnu.edu.cn
Dr. B den Albela, Laurent Bonneviot
Laboratoire de chimie, Ecole Normale Supérieure de Lyon, Institut de Chimie de Lyon
Université de Lyon
46 Allée d'Italie, 69364 Lyon cedex 07, France
E-mail: laurent.bonneviot@ens-lyon.fr

KEYWORDS: self-assembly, hybrid materials, nanoparticles, porosity, Solid acid catalysis.

ABSTRACT: Mesoporous nanospheres are highly regarded for their applications in nanomedicine, optical devices, batteries, nanofiltration and heterogeneous catalysis. In the latter field, the dendritic morphology favoring molecular diffusion is a very important morphology known for silica but not yet for carbon. A one-pot, easy and scalable co-sol-gel route using the triphasic resol-surfactant-silica system is shown to yield the topologies of the title by inner radial phase speciation control on a mass-transfer limited process depending on the relative polycondensation rates of the resol polymer and silica phases. The trick was the use of polyolamines having different catalytic activities on each hard phase polycondensation. The self-entanglement of phases is produced at the $\{O^-, S^+, I\}$ organic-surfactant-inorganic interface. Mono- and biphasic mesoporous sister nanospheres of carbon and/or silica are derivatized from each mother nanospheres and called "syntactic" as having similar size and mirrored morphologies. Comparing these "false twins" or yin and yang mesoporous

nanospheres functionalized by sulfonoyl groups evidences the superiority of the dendritic topologies and the absence of a shell on the diffusion-controlled catalytic alkylation of *m*-cresol.

1. Introduction

A plethora of living systems such as bones, teeth and shells of various compositions inspire chemists to develop entangled inorganic-organic phases.^[1] In diatoms, highly pure biosilica is produced selectively by specific enzymes activating the Si-OH polycondensation.^[2] These catalytic sites mimicked here by polyolamines (POA) allow fast condensation even around pH neutrality.^[3] The molding amphiphilic phospholipids of membranes are replaced by single long chain alkyltrimethylammoniums, as in the syntheses of the emblematic mesostructured porous silicas MCM-41 and MCM-48.^[4] The structural control is obtained on both array and size of pores, combining hard and soft matter like in the biogenic materials.^[1a, 1j, 3-5] Spontaneous soft-soft and hard-hard entanglements of matter reported in tubular vesicles, in de-mixing microphases and in ceramics remain rare.^[6] Not yet understood nor described in Mother Nature, spontaneous assembly of three phases is even more challenging and scarce.^[7] The easy-to-perform synthesis proposed here concerns the class I type of structural nanohybrids adopting a variety of inner topologies and pore arrays. It proceeds from the spontaneous entangled growth of two hard phases – resorcinol and silica – mediated by soft matter – a water-surfactant phase.

The impressive progress in sol-gel chemistry of silica on the design of porous nanoparticles in the last 20 years was mirrored by that of porous carbon nanoparticles with increasing control on shape, topology, size and pore structure.^[8] Very open stellar porosity in silica nanoparticles are obtained introducing specific catalytic additives or playing with interfacial growth control.^[3, 9] Resorcinol- or phenol-formaldehyde condensation self-assembled with a neutral surfactant yields also monodisperse nanospheres using high

dilutions.^[10] Surprisingly, the addition of silica precursors to styrene or to resol and phenol-formaldehyde polymer precursors leads to new morphologies with a loss on the control of the size.^[7, 10h, 10n] Monodispersed hollow carbon-silica porous nanospheres were recently produced by one-pot synthesis by the group of Cao et al. using either classic thermal activation or microwave assisted.^[11] Concomitant control on morphology, size and porosity on polymer-silica nanohybrids can also be obtained by co-assembly of preformed resol and silica nanophases inside films formed by the evaporation induced self-assembly process (EISA).^[7b] Hard templating, high dilution, water oil emulsion or any sequential routes are discarded in the present work to keep the focus on easy up scaling. We propose instead to grow together polymeric and siliceous hard nanophases with positively-charged micelles in conditions adapted from those of the group of Cao with in addition the use different specific catalytic amines for the control on the relative rate of silica and resol condensations.^[11]

We will discover from transmission electron microscopy (TEM) that their inner structure is fingerprinting a mutual though asymmetrical action of one phase on the other: the nascent silica phase scaffolding the growth of the resol phase. The former considered as *yang* and the latter as *yin* emphasizes that they are not really twin phases as we shall see. The word “syntaxy” is meant to designate any mechanism by which two solid phases are grown by self-assembly from their molecular precursor leading therefore to “syntactic” nanophases. It is built from two ancient Greek words *sun* for syn- meaning “together” and *tikto* for -taxy or -taxis meaning “to give birth and/or to grow” (SI). Among three topologies cited in the abstract, two are new and all are thoroughly investigated not only entangled but also separated. The word topology is related here to any specific speciation of composition or density pattern, while pore array is related to the pore shape and distribution, as we shall observe from energy dispersive X-ray (EDX) analysis mapping and TEM images (SI). The void between the *yin* and the *yang* solid phases will be characterized using N₂ physisorption. The effect of the microporous silica shells on molecular diffusion-limitation will be evidenced comparing

nanospheres of various topologies as supports for the acid catalyzed *tert*-butyl alkylation of *m*-cresol.

2. Results and Discussion

2.1. A scalable synthesis of hybrids materials and their derivatized biphasic and monophasic porous sister phases.

The polymer-surfactant-silica – PSS – mesoporous nanospheres – MNS – were obtained by hydrothermal treatment at 80 °C of slightly basic solutions prepared at room temperature from ethanol and water as co-solvents, cetyltrimethyl ammonium bromide – CTAB – as surfactant, tetraethylorthosilicate – TEOS – as silica precursor, a resorcinol-formaldehyde mixture – RF – as resol precursor and a catalytic amine x ($= 1-3$); 1 = TEAH₃ (triethanolamine), 2 = AHMPD (2-amino-2-(hydroxymethyl)-propane-1,3-diol) and 3 for ammonia (Fig. 1). After filtration and drying for 24 h at 80 °C, ethanol free polymer/water-surfactant/silica triphasic nanospheres denoted as PSS-MNS- x were recovered and freed from the surfactant by extraction yielded then biphasic polymer-silica hybrids – PS – noted PS-MNS- x . Carbonization of PSS or PS hybrids respectively, yielding the carbon-silica hybrids *CS-MNS- x and CS-MNS- x (derivatization sequence and sample the nomenclature in Fig. 1). Etching the silica nanophase yielded the corresponding polymer or carbon *in* nanospheres P-MNS- x , *C-MNS- x and C-MNS- x , while their *yang* silica counterpart S-MNS- x were obtained after calcination in air. Note that the composition of the mother liquor was very close to that of regular MCM-41 synthesis used previously to investigate the surfactant-silica system.^[3] It differs mainly from a higher dilution (3.5 times), the addition of ethanol and a surfactant/silica ratio twice higher to reach the conditions for the targeted dendritic topology. Adding resorcinol and aldehyde resulted to a mother liquor of similar composition than that used to produce hollow spheres by the group of Cao.^[7a] The main difference was the nature of the amine while the concentration of resorcinol was three times increased to finally obtain the

dendritic morphology. The polymer and silica yields for the synthesis of PSS-MNS-1 were 55 and 43%, respectively and 44 and 63% for the other two amines ($x = 2$ and 3). These syntheses are very robust and can be scaled up to the kilogramme scale (see experimental part).

2.2. Electron microscopy investigation: an amine dependent topology.

The size and shape of the hybrid systems were investigated using scanning electron microscopy (SEM) while monophasic systems revealed a better inner contrast of their topology and pore array using TEM (Figure 1). According to SEM images, amine 1 favored a narrow distribution of sizes, with nanospheres comprised between 100 and 150 nm (Figure 1a). With amine 1, the silica nanospheres possessed a uniform (U) dendritic (De) topology, with pores having a thin finger-like wall (dendrite) and external apertures ranging from 9 to 17 nm (nomenclature in SI, Figure 1d, 2a, and Table 1). This so-called U-De silica morphology had in common with its carbon counterpart the size and the uniform topology. However, the latter exhibited rather flat walls with voids that can be view as a perforated-veil denoted U-Pv (Figure 1g, 2d). Grown in very similar conditions without resol precursors, silica adopted a raspberry type of pore array, U-Rb (Figure 5Sb). Nonetheless, the actual U-De topology is more alike the stellar morphology (St) obtained also without resol precursor while using tosylate as counter-ions instead of bromide.^[3] The main difference consists to thicker wall at the center than at the periphery leading to a slightly denser core and a wide open outer part in contrast with U-De (Figure 2g).^[3]

In comparison, amines 2 and 3 yielded larger nanospheres of *ca.* 400 nm and *ca.* 600 nm, respectively (Figure 1b, 1c and Figure S1B). The nanospheres of S-MNS-2 exhibited a core-shell-corona (CSC) topology with a dense shell, 50-70 nm thick, unexpectedly located inside of the nanosphere with low density cores and coronas (Figure 1e, 2b). The S-MNS-3 exhibited a typical core-shell (CS) topology (Figure 1f, 2c). In SMNS-2 and -3, the shells presented center-radial micropores with diameters smaller than 2 nm while the cores were

much less structured, particularly in S-MNS-2 (Figure 2b and 2c). In comparison to the *yang* S-MNS-*x* nanophases, the *yin* carbon counterpart, C-MNS-*x*, exhibited similar inner topologies with an inverted contrast and, definitively, a less defined pore structure (Figure 1g, h and i). These observations are consistent with the *yin* being entangled together with the *yang* nanophase, each adopting complementary inner structures, called *syntaxic*.

2.3. Elemental mapping EDX analysis: growth with competitive mass transfer between precursors.

Mapping the composition using energy dispersive X-ray (EDX) analysis indeed confirmed that both C and Si atoms were present in each hybrid nanoparticle whatever the base at play (Figure 3). The map of Si atoms matching well that of O atoms traced the SiO₂ nanophase while that of C atoms traced the resol nanophase (Figure 3, row 5). No phase segregation between particles could be detected by EDX in CS-MNS-1. Nonetheless, a close look at the periphery where silica dendrites showed more clearly that the position of the carbon phase did not fully coincide with the position of the SiO₂ phase suggesting that one phase was wrapping up the other (Figure 3, column 1). Conversely, the elemental mapping of CS-MNS-2 and -3 confirmed some phase speciation, indeed, the dense shells observed on the TEM images were silica-rich zones. This is in striking contrast with the EDX fingerprint of hollow spheres where both phases are equally present in the shell while the core appears empty.^[11a] This is consistent with a faster development of the resol network than in C-MNS-1, which was favored over that of silica at the early stage of the synthesis. The presence of a dense shell inside the nanosphere in CS-MNS-2 evidenced two inversions of the tendency. The first one took place at an intermediate stage of the synthesis while the second at the last step of the growth, producing a less dense corona. Using ammonia instead produced this inversion only at the very end of the synthesis, generating a silica dense outer shell and, therefore, no corona (CS-MNS-3, Figure 3, column 3). The phase speciation in the core can be assigned to a temporary faster condensation rate of the polymer phase, producing a

WILEY-VCH

concentration gradient of its precursors around the nucleus. With time, the increasing gradient becomes enough disfavoring for the polycondensation rate of the silica takes over that of the resol. In turn, during the formation of the silica-rich shell, this was now the built up of the concentration gradient in silica precursors that brought the possibility to reach a second breaking point before the end of the synthesis. This occurs in S-MNS-2 where a carbon-rich corona can be formed before the end of the synthesis. In other words, a mass transfer limitation takes place as the molecular precursors have to diffuse among micelles that, in turn progressively stick one with another during the growth. Then, one understands why the relative rate of polycondensation of each phase is a crucial parameter to reach the composition homogeneity. In fact, polyolamine 2 has a lesser catalytic effect than polyolamine 1 and generates also a higher pH, both criteria are favoring of the resol condensation. This slower silica polycondensation results to a decrease of its concentration in the core. Ammonia is even a worse catalyst than 2 for silica condensation generating also higher pH and pushed the trend further explaining the silica-rich outer shell (pH and pK_A in Table S1). As the pH itself decreases gradually down to a final value of 8.1 tuning both phase concentrations all along the synthesis is a very subtle game ($\sim 1.2\%$ residual deprotonation of resorcinol, Table S1).^{[1], [2]} The mass balance in the triphasic nanospheres is also consistent with this point of view as the presence of a silica-rich shell is marked by a higher proportion of this phase in the composition (resol/surfactant/silica mass ratio of 18/57/23 in PSS-MNS-1 and 15/49/36 in PSS-MNS-2 and -3, measured from TGA, Figure S2). The formation of the CSC topology was a lucky gift as it brought us a lot of insights on the mechanism. The subtle competitive mass transfer between both hard phases precursors during the growth process precludes any precise prediction on the radial composition and fully justifies a trial and error approach, guided by the effect of the parameters described here (Fig. S4).

2.4. The leading drive of the silica nanophase scaffolding the resol nanophase.

Changing the amine concentration or the solid phase precursor concentration indeed affected both topology and pore array (Fig. S3-S5). The uniform topology of PSS-MNS-1 nanospheres was lost at low TEAH₃ concentration, leading an inverse core-shell speciation of composition in comparison to PSS-MNS-3 (Fig. S3 and S4). The rational explanation is found in the decrease of pH disfavoring further the polycondensation of the resol phase over that of the silica phase, the latter still taking advantage on the few of catalytic amines *I* still present. Conversely, too high TEAH₃ concentrations generating too high pH favored the nucleation of each phase independently forming nuclei with heterogeneous composition. In the present condition of concentration and pH that differ slightly from our previous investigation, we verified that this is effectively the U-Rb topology that is produced (Fig. S5b).^[3] Conversely, in the absence of silica, the resol polymer is known to form large and non-porous spheres of *ca.* 1.0 μm , which we also confirmed in our particular conditions (Fig. S5d).^[10d] Consistently, carbon-rich areas in CS and CSC topologies developed less defined porosity than silica-rich areas. The structural synergy observed between the entangled phases is additional fingerprint of the syntaxy principle while the strong topology dependence on precursor concentration further support the hypothesis of diffusion controlled nucleation process starting from very small clusters of micelles-precursor composites.

2.5. A class I nanohybrid: two hard nanophases sandwiching a soft hard phase of few nm thick.

The porosity of the surfactant-free hybrid nanospheres was confirmed by N₂ sorption isotherms (Fig. S6 and S7, and Table 2). The presence of the shells was the cause of the porosity loss in PSS-MNS-*x* (*x* = 2 or 3), which was assigned to pore plugging by the weakly reticulated resol phase (see FT-IR and ¹³C NMR, Fig. S8 and S9). The carbonization solved this problem revealing large surface areas (300-800 m^2g^{-1}) and large pore volumes (1 to 1.7 ml/g) (Table 2), consistent with the different topologies (Fig. 2).

The volumetric surface areas (surface developed per unit of volume) that better describe the spatial occupancy are indeed rather close, supporting the idea that both entangled nanophases are facing one to the other through a common interface (Fig. 4A and Table 2). Strikingly, the well-defined pores of 5 nm in PS-MNS-1 evidenced that both *yin* and *yang* nanophases were split apart by a distance that shrank by *ca.* 20% after carbonization (Fig. 4). In addition, the absence of any signal at 64 ppm after mild carbonization at 350 °C excluded the formation of covalent Si-O-C bridges between both hard nanophases, advocating for the formation of a class I type of nano-hybrids (Figure S9).^[7b]

2.6. Topology dependence on a diffusion-controlled catalytic reaction.

Applying these nanospheres as support for a reaction of industrial importance was appealing particularly to test whether dendritic morphologies were advantageous. We chose the catalytic *tert*-butyl alkylation of *m*-cresol that run in liquid media where molecular diffusion-limitation is crucial. Then, the monophasic X-MNS-*x* nanospheres (X = C or S) were compared to benchmark heterogeneous catalysts for this reaction (Fig. 4B). Their surfaces were functionalized with acidic sulfonate groups, leading to S-MNS-*x*-SO₃H and C-MNS-*x*-SO₃H nanospheres (level of sulfonation available in SI).^[10r, 13] The references were the emblematic acid heterogeneous catalysts ZSM-5 (Si/Al = 50) and USY-1, 2 and 3 (Si/Al = 5.2, 12 and 36.9, respectively) (Table S2). The highest conversion, ~ 60 and 66%, using S-MNS-1-SO₃H and C-MNS-1-SO₃H, respectively was attributed to their highly open porosity, being even better than USY-2 and 3, presenting themselves large voids created during the dealumination treatment (Table S2 and Fig. S10). By contrast, S-MNS-2-SO₃H and, particularly S-MNS-3-SO₃H, were much less active and compared better with the microporous ZMS-5 and USY-1 presenting mainly micropores and the largest diffusion limitation. The carbon *yin* nanospheres C-MNS-*x*-SO₃H possessing no dense shells exhibited intermediary conversions scaling better with their exposed surface area (Table S2, Fig. 5). The more advantageous selectivity/conversion ratio obtained with the silica support is

probably due to its larger organic coverage and its higher hydrophobic surface than that of the sulfonated carbon nanospheres. This clearly shows that shell-free and wide-open pore topologies are highly favorable for heterogeneous catalysis, as they minimize molecular diffusion-limitation. After four cycles of use of C-MNS-1-SO₃H, the catalyst still maintains a high activity and selectivity (Fig. S11), and the SEM observations show that their morphology and structure are maintained after long-term use (Fig. S12). Conversely, the presence of the silica shell is certainly more favorable for other applications like electrical storage or drug delivery, though biocompatibility remains to investigate.^[1i, 8b, 14]

2.7. Syntactic entanglement at the {*O*⁻, *S*⁺, *I*} interface.

The well-known biphasic silica-surfactant self-assembly mechanism is likely to be extrapolated to the present three-body mechanism.^[6a] In the former, the silicate oligomers condense into nanoflakes.^[3] These flakes merge together crosslinking the micelles one with the other. Different morphologies of silica nanospheres cited above are then produced, depending on the micelle coverage (Fig. 1g-i). In the three-body mechanism, the resorcinolate anions (pH_i ~ 10.4, Table S2) are likely adsorbed on the micelles together with the silica precursors.^[11a] The latter first form silica-nanoflakes, catalyzed by the amine *I* (step I of the synthesis, Fig. 5). These flakes facilitate the micelle merging and also increase the local concentration in resol precursors, favoring the initiation of the resol polycondensation (step II, Fig. 5). The growing silica-network is progressively mirrored by the resol-network, with a water-surfactant layer in between (step III, Fig. 5). Note that a lower coverage by silica-flakes is expected to generate lower density of hard matter, i. e., larger pores. This is effectively observed here changing polyolamine 2 for polyamine *I* leading to larger pores of 9 nm in PS-MNS-2 (Fig. 4A). This mechanism explains how the *yang* silica nanophase triggers the nucleation and scaffolds the shape of the *yin* resol nanophase, both adopting syntactic forms, as a hand fits a glove (Fig. 5). It explains also why the solid phases grow separately,

split by a distance defined by the water-surfactant layer. This characteristic distance of 5 nm in the as-made material matches well with the 14 nm of the single nanophases assuming that the pore wall thickness of the eliminated phase was approximately 4 nm (Fig. 4C). Note that the same pore wall thickness in PS-MNS-2 explains also the shift of pore size from 8-9 nm to 20-22 nm in the single phases, P- or C-MNS-2 and S-MNS-2. In the as made PSS-MNS-x materials, this interface is denoted as $\{O^-, S^+, I\}$ according to the notation for the surfactant-inorganic association of matter O^- designating the organic phase.^[15]

2.8. Co-assembly and syntaxy, two different strategies of synthesis.

Synthesizing triconstituent nanospheres by co-assembly is a multi-pot approach where both hard phases are pre-condensed at different pH's. The organic and inorganic phases are then mixed together before introducing the neutral surfactant, S^0 .^[7b] The templated self-assembly takes place at this last step at, what we propose to call, a $\{S^0, (O-I)^0\}$ interface. Both organic and inorganic phases sharing covalent C-O-Si bridges led to a class II type of hybrid. As a consequence, eliminating one of the nanophases generates pores inside the walls of the remaining phase that are smaller than those templated by the surfactant, in sharp contrast with the present case. Though co-assembly and syntaxy are both belonging to the family of templated self-assembly processes, the former operates on preexisting hard nanophase(s) while the latter takes place with molecular precursor(s). Syntaxy belongs to the templated molecular self-assembly in the classification of Whitesides.^[16]

2.9. Comparison with other one-pot polymer-surfactant silica systems.

In different conditions set for one pot synthesis than the co-assembly route, Zhang *et al.* discovered that adding silica to the resorcinol-CTAB system lead to unprecedented variety of shapes and topologies – tubular to spherical – and inner topologies – hollow and yolk-shell.^[7a]
^[11] Applying solvent adjustment to the one-pot approach led also Hou *et al.* to control the size of hollow nanospheres while Zhou *et al.* shortened the ageing time to 1 hour using the assistance of a microwave irradiation.^[11] To target the U-De topology, the resorcinol was

three times more concentrated and the ammonia was replaced by a polyolamine. Surprisingly, coming back to ammonia (amine 3) with this high resorcinol concentration led us to the CS polymer-rich core morphology instead of hollow polymer-silica nanohybrids.^[11a] This indicates that increasing three times the concentration of resorcinol completely change the kinetics and the topology. This shows how much these syntheses are sensitive.

The synthesis interface proposed here is certainly the same in the hybrid nanospheres in both cases. In neither absence of specific information on the type of nanohybrid (I or II) nor any comparison between the porosity of the monophasic and the biphasic systems preclude any further comparison. The difference is the mechanism. We advocate for a nucleation growth starting from individual micelles decorated by the both solid phase precursors. It explains the evenly distributed phases in the U-De topology and the radial speciation from the center of the nanosphere for CSC and CS morphologies. Conversely, the size, the shapes and the hollow core are preferentially described by precursors diffusing from the outside to the inside of already formed large aggregates of micelles (emulsion seen few minutes after formaldehyde addition, before the introduction of TEOS). As this mechanism is not compatible with our observations, the higher concentration of resorcinol may disfavor their mechanism by triggering ours. More investigations are still needed to clarify the situation.

2.10. Syntax among the other strategies of templated synthesis.

The mechanism of formation of the present *yin-yang* entangled pairs of nanophases is obviously related to the nano objects of different shapes produced by the group of Cao.^{19, 46-47} To clarify the situation with the solid phases obtained by the co-assembly route proposed by the group of Zhao,^[7b] the molecularly self-assembled material needed a specific qualification that we call syntactic. Semantically, this principle includes biphasic soft-hard systems and therefore the synthesis of the emblematic MCM-41 and SBA-n.^[3-6, 8f, 15] Practically, one may exclude the biphasic systems that leave behind only one solid phase and no syntactic sister phases as a complementary signature of the mechanism. In contrast, a triphasic hard-soft-hard

system produces for a single morphology at least 3 syntactic solid phases (here up to 7 from the derivatization scheme of fig. 1). This is the analysis of the set of syntactic solid phases makes the difference with the co-assembly route, which *de facto* is not syntactic (see above). Hard templating is another pathway that is also non-syntactic like the liquid crystal templating route assuming a liquid preorganization of the template.^[17] Interestingly, the folded sheet material (FSM) resembling to MCM-41 is derivatized from a lamellar kanemite swelled by cationic surfactant.^[17b] It is therefore also non-syntactic and could be classified as a templated phase transition (TEPT) route. Our classification based on mechanistic specificity complete the strategic map proposed lately by Liu *et al.*^[10r]

3. Conclusions

It has been shown that the catalytic control on the relative rate of polycondensation of the two hard phases in the co-sol-gel synthesis of the resol-CTAB-silica system lead to new morphologies. Using amine catalyzing specifically the silica condensation at the expense of the resol polycondensation allowed us to move from the uniform dendritic, to phase partitioned core-shell-corona and core-shell topologies. This radial speciation is typical of a mass transfer limitation of the solid precursor during the growing process explaining why a variety of topologies can be observed. To our knowledge, the derivatization of the dendritic hybrid into the carbon sister nanosphere is up to now the sole route available to generate monodisperse dendritic carbon nanospheres. The core-shell-corona is also a novel topology not only for carbon but also for silica. The proposed mechanism is comparable to that of the biphasic surfactant-silica system where silica drives the porosity of the polymer phase, acting as a co-temple together with the surfactant. This asymmetry led to “false twin” *yin* and *yang* pair of phases. This actual three-body system takes place at an organic-surfactant-inorganic $\{O^-, S^+, I\}$ interface and led us to define a new principle called *syntaxy*. The variety of topologies obtained for two hard phases at a time each of the derivatized in several mono or biphasic sister phases is particularly attractive for comparative investigations at the nanoscale.

It is exemplified here in the diffusion controlled catalytic alkylation of *m*-cresol where the shell free phases are the most active and selective. The present mechanism likely amenable to other systems paves the way for the syntheses of novel multiphasic nanohybrids, and novel applications in chemistry, material sciences, and nanomedicine.

4. Experimental Section

Syntheses of entangled resol-CTA-silica triphasic nanospheres from polyolamine 1: The dendritic mesoporous resol-CTA-silica nanospheres (PSS-MNS-1) were synthesized using a one-pot soft-templating method (Fig. 1). A typical synthesis of dendritic PSS-MNS-1 was performed as follows: triethanolamine (TEAH₃) aqueous solution (10.6 g; $pK_a = 7.8$) was mixed with a solution containing resorcinol (5.0 g), CTAB (5.0 g), absolute ethanol (EtOH, 200 mL), and deionized water (500 mL), then stirred for 0.5 h. Subsequently, formaldehyde solution (5.0 mL, 37 ~ 40 wt%) was added and continuously stirred for 2 - 5 min. Then TEOS (25 mL) were added to the reaction solution and stirred for 24 h at room temperature. The final molar composition of the sol-gel mixture is 1.0 SiO₂ : 0.40 Resorcinol : 0.75 HCHO : 0.12 CTABr : 0.66 TEAH₃ : 30 C₂H₅OH : 248 H₂O. The reaction mixture was further heated for 24 h at 80 °C under a static condition in a Teflon-lined autoclave. The obtained dendritic mesoporous resin-silica composite nanospheres were recovered by filtration and air-dried at 80 °C overnight yield 16 g and were denoted as for with 1 standing for the use of TEAH₃ as alkali source (see below for the other bases). The resol/silica/surfactant/water mass ratio was ca. 18/59/23, according to TGA see Fig. S2. The yields in resol and in silica were 55 and 43%, respectively. A successful up scaling using a 20L vessel demonstrated that a 60 L vessel filled at 75% (45 L) is need for 1 Kg of PSS-MNS-1(i.e. 410 g of dry PS-MNS-1).

Syntheses of MNS using either amine 2 or 3: Core-shell-corona (CSC) or core-shell (CS) mesoporous hybrid nanospheres were formed and designated PSS-MNS-2 (or -3) when

WILEY-VCH

aqueous 2-amino-2-(hydroxymethyl)-propane-1,3-diol (2 for AHMPD, $pK_a = 8.1$) and ammonia (3 = $\text{NH}_3 \cdot \text{H}_2\text{O}$, $pK_a = 9.2$) were used instead of TEAH_3 for the same solution composition. The yield in air-dried as-made hybrid nanosphere was 14.9 and 15.1 g for amine 2 and 3, respectively. The resol/silica/surfactant/water mass ratio was *ca.* 15/49/36, according to TGA see Fig. S3. The yield was respectively 44 and 63% in resol and in silica producing *ca.* 940 g of PSS-MNS and 550 g of dry PS-MNS in the same up scaling conditions given for 1Kg of PSS-MNS-1.

Syntheses of C-MNS-x and S-MNS-x carbon or silica single-phase nanospheres: The triphasic nanospheres PSS-MNS-x ($x = 1, 2, 3$) were carbonized in inert atmosphere using a tubular furnace, raising the temperature ($3^\circ\text{C}/\text{min}$) up to 900°C and maintaining this temperature for 3 h under a N_2 gas flow. After cooling, the silica was removed by immersing the obtained carbon-silica composites in 10 wt% HF aqueous solution at room temperature for 24 h, followed by washing with water. The mesoporous carbon nanospheres were dried overnight. When the surfactant was chemically removed before carbonization, the solid was denoted C-MNS-x while direct carbonization of the as-made nanosphere led to the material denoted as *C-MNS-x. The dendritic mesoporous silica nanospheres S-MNS-x were obtained by direct calcination of PSS-MNS-x at 550°C for 6 h in air.

Material characterizations: The X-ray diffraction (XRD) patterns were collected on a Rigaku Ultima IV X-ray diffractometer with Cu K_α radiation ($\lambda = 1.5405 \text{ \AA}$) at 40 kV and 40 mA. Nitrogen adsorption-desorption isotherms were recorded at 77 K on a Quantachrome (O2108-KR-1) after activating the sample under vacuum at 473 K for at least 10 h. The SEM images were captured using a Hitachi S-4800 microscope. TEM analyses were performed using a JEOL 2010F microscope equipped with a field emission gun and operating at 200 kV. Point by point Energy dispersive X-ray spectroscopy (EDS) providing the concentration profiles of

oxygen, silicon and carbon atoms through the nanospheres were measured using the transmission electron microscope in scanning mode. FT-IR spectra were recorded on a Nicolet Fourier transform infrared spectrometer (NEXUS 670) diluting the sample in a fine KBr powder that was pressed into pellet. Solid ^{13}C CP MAS NMR measurements were collected using a VARIAN VNMRS-400WB spectrometer. For ^{13}C (100.6 MHz), a $6\ \mu\text{s}$ ($\theta = \pi/2$) pulse was used with a repetition time of 3 s.

Preparation of C-MNS- x -SO₃H and S-MNS- x -SO₃H catalysts: The preparation of X-MNS- x -SO₃H catalysts (X = S for silica or C for carbon, $x = 2$ or 3) followed a recipe described in ref. 42. The sulfonation of the 0.3 g mesoporous carbon nanospheres (C-MNS- x) were carried out in a Teflon container set in a Teflon-lined autoclave where the powders were contacted with the vapor from 5 mL 50% SO₃/H₂SO₄ at 383 K for 24 h. The sulfonated samples, X-MNS- x -SO₃H, were washed with hot distilled water ($> 353\ \text{K}$) and filtrated until no sulfate ions were no longer detected in the filtration water, and dried at 373 K overnight in air. Sulfonic acid functionalized mesoporous silica nanospheres S-MNS- x -SO₃H were prepared as follows: the S-MNS- x sample (1 g) was dried at 120 °C, and then 3-mercaptopropyltriethoxy-silane (2 mmol) in dry toluene (40 mL) was introduced. The mixture was refluxed for 6 h, and the solid was filtered off, washed with toluene and acetone, and air-dried. The -SH groups were converted into -SO₃H groups by oxidation using a mixture of aqueous H₂O₂ (30%, 10 mL) and CH₃OH (30 mL) for 6 h at a reflux temperature. After filtration and washing with water and ethanol, the sample was then acidified in 2.0 M HCl solution for 1 h, followed by washing with water until neutral pH and drying at 100 °C for 6 h. The number of acid sites were measured from NH₃ TPD desorption (Table S2). For control experiments, zeolite catalysts of ZSM-5 (Si/Al = 50), and USY-1, 2 and 3 with varied Si/Al molar ratios (Si/Al = 5.2, 12 and 36.9) and tunable hierarchical porosity were obtained commercially. All the zeolites were

converted into proton type by ion-exchanged with NH_4NO_3 solution followed by calcination at 773 K for 6 h.

Catalytic test: The alkylation reaction of *m*-cresol and *tert*-butyl alcohol was performed by stirring the mixture of 0.1 g catalyst, 4.0 g *m*-cresol and 3.4 g *tert*-butyl alcohol at 403 K for 2 h. The product identification was obtained from gas chromatograph-mass spectrometer (Agilent HP6890/5973N) calibrated with pure molecules, that are all commercially available. Precise quantification was obtained from a Shimadzu 14B gas chromatograph equipped with an OV-1 capillary column.

Supporting Information

Supporting Information is available from the Wiley Online Library or from the author.

Acknowledgements

The research was conceived and designed by ZK and WP with the follow up of LB. The latter proposed also the mechanism and the nomenclature, designed the figures and wrote the article with the assistance of ZK and BA. LB dedicates this paper to his inspiring mentors, Profs. Jacques Livage and Michel Che. This work was supported by the NSFC (21373004, 21573074 and 21533002), the CAS key laboratory of Low-Coal Conversion Science & Engineering and JoRISS program. On the French side, the support came from the Joint Research Institute for Science and Society founded by ECNU and ENS de Lyon, and by the Auvergne-Rhône-Alpes Region together with the French Ministry of European and Foreign Affairs via an ARCUS-China grant. KZ thanks ENS de Lyon for a temporary position as invited professor in France. LB also acknowledges the Chinese Government for the very helpful Higher End Foreign Expert position at ECNU. Prof. Dongyuan Zhao from Fudan University is acknowledged for his precious advices on the manuscript. We thank also Dr. Pierre Avenas for guiding us on building the word “syntaxy”.

Received: ((will be filled in by the editorial staff))

Revised: ((will be filled in by the editorial staff))

Published online: ((will be filled in by the editorial staff))

References

- [1] a) S.-H. Wu, C.-Y. Mou, H.-P. Lin, *Chem. Soc. Rev.* **2013**, 42, 3862; b) C. Sanchez, P. Belleville, M. Popalld, L. Nicoleab, *Chem. Soc. Rev.* **2011**, 40, 696; c) C. Sanchez, H. Arribart, M. M. G. Gille, *Nat. mater.* **2005**, 4, 277; d) C. Sanchez, C. Boissiere, S. Cassaignon, C. Chaneac, O. Durupthy, M. Faustini, D. Grosso, C. Laberty-Robert, L. Nicole, D. Portehault, F. Ribot, L. Rozes, C. Sassoeye, *Chem. Mater.* **2014**, 26, 221; e) L. Han, S. Che, *Chem. Soc. Rev.* **2013**, 42, 3740; f) C. Gao, S. Che, *Adv. Funct. Mater.* **2010**, 20, 2750; g) C. Argyo, V. Weiss, C. Bräuchle, T. Bein, *Chem. Mater.* **2014**, 26,

- 435; h) K. Möller, T. Bein, *Chem. Mater.* **2017**, 29, 371; i) Y. Chen, H.-R. Chen, J.-L. Shi, *Acc. Chem. Res.* **2014**, 47, 125; j) S. Mann, D. D. Archibald, J. M. Didymus, T. Douglas, B. R. Heywood, F. C. Meldrum, N. J. Reeves, *Science* **1993**, 261, 1286.
- [2] a) M. Hildebrand, B. E. Volcani, W. Gassmann, J. I. Schroeder, *Nature* **1997**, 385, 688; b) K. Shimizu, J. Cha, G. D. Stucky, D. E. Morse, *Proc. Natl. Acad. Sci.* **1998**, 95, 6234.
- [3] K. Zhang, L.-L. Xu, J.-G. Jiang, N. Calin, K.-F. Lam, S.-J. Zhang, H.-H. Wu, G.-D. Wu, B. Albel, L. Bonneviot, P. Wu, *J. Am. Chem. Soc.* **2013**, 135, 2427.
- [4] C. T. Kresge, M. E. Leonowicz, W. J. Roth, J. C. Vartuli, J. S. Beck, *Nature* **1992**, 359, 710.
- [5] a) J. Livage, *C. R. Palevol* **2009**, 8, 629; b) S. Chiruvolu, H. E. Warriner, E. Naranjo, S. H. Idziak, J. O. Radler, R. J. Plano, J. A. Zasadzinski, C. R. Safinya, *Science* **1994**, 266, 1222.
- [6] a) A. Firouzi, D. Kumar, L. Bull, T. Besier, P. Sieger, Q. Huo, S. Walker, J. Zasadzinski, C. Glinka, J. Nicol, a. et, *Science* **1995**, 267, 1138; b) Y. Waku, N. Nakagawa, T. Wakamoto, H. Ohtsubo, K. Shimizu, Y. Kohtoku, *Nature* **1997**, 389, 49.
- [7] a) X. Zhang, Y. Li, C. Cao, *J. Mater. Chem.* **2012**, 22, 13918; b) R. Liu, Y. Shi, Y. Wan, Y. Meng, F. Zhang, D. Gu, Z. Chen, B. Tu, D. Zhao, *J. Am. Chem. Soc.* **2006**, 128, 11652.
- [8] a) C. E. Fowler, D. Khushalani, B. Lebeau, S. Mann, *Adv. Mater.* **2001**, 13, 649; b) Y.-S. Lin, N. Abadeer, K. R. Hurley, C. L. Haynes, *J. Am. Chem. Soc.* **2011**, 133, 20444; c) D. Niu, Z. Liu, Y. Li, X. Luo, J. Zhang, J. Gong, J. Shi, *Adv. Mater.* **2014**, 26, 4947; d) C. Urata, Y. Aoyama, A. Tonegawa, Y. Yamauchi, K. Kuroda, *Chem. Commun.* **2009**, 5094; e) A. B. D. Nandiyanto, S.-G. Kim, F. Iskandar, K. Okuyama, *Microporous Mesoporous Mater.* **2009**, 120, 447; f) D. Zhao, J. Feng, Q. Huo, N. Melosh, G. H. Fredrickson, B. F. Chmelka, G. D. Stucky, *Science* **1998**, 279, 548.
- [9] D. Shen, J. Yang, X. Li, L. Zhou, R. Zhang, W. Li, L. Chen, R. Wang, F. Zhang, D. Zhao, *Nano Lett.* **2014**, 14, 923.
- [10] a) Y. Fang, D. Gu, Y. Zou, Z. Wu, F. Li, R. Che, Y. Deng, B. Tu, D. Zhao, *Angew. Chem. Int. Ed.* **2010**, 49, 7987; b) C. Liang, Z. Li, S. Dai, *Angew. Chem. Int. Ed.* **2008**, 47, 3696; c) A.-H. Lu, W.-C. Li, G.-P. Hao, B. Spliethoff, H.-J. Bongard, B. B. Schaack, F. Schüth, *Angew. Chem. Int. Ed.* **2010**, 49, 1615; d) J. Schuster, G. He, B. Mandlmeier, T. Yim, K. T. Lee, T. Bein, L. F. Nazar, *Angew. Chem. Int. Ed.* **2012**, 51, 3591; e) J. Liu, S. Z. Qiao, H. Liu, J. Chen, A. Orpe, D. Zhao, G. Q. Lu, *Angew. Chem. Int. Ed.* **2011**, 50, 5947; f) J. Liu, T. Yang, D.-W. Wang, G. Q. Lu, D. Zhao, S. Z. Qiao, *Nat. Commun.* **2013**, 4, 2798; g) K. Möller, J. Kobler, T. Bein, *Adv. Funct. Mater.* **2007**, 17, 605; h) Z.-A. Qiao, B. Guo, A. J. Binder, J. Chen, G. M. Veith, S. Dai, *Nano Lett.* **2013**, 13, 207; i) J. Tang, J. Liu, C. Li, Y. Li, M. O. Tade, S. Dai, Y. Yamauchi, *Angew. Chem. Int. Ed.* **2015**, 54, 588; j) J. Zhang, Z.-A. Qiao, S. M. Mahurin, X. Jiang, S.-H. Chai, H. Lu, K. Nelson, S. Dai, *Angew. Chem. Int. Ed.* **2015**, 54, 4582; k) K. Wang, L. Huang, S. Razzaque, S. Jin, B. Tan, *Small* **2016**, 12, 3134; l) H. Tian, Z. Lin, F. Xu, J. Zheng, X. Zhuang, Y. Mai, X. Feng, *Small* **2016**, 12, 3155; m) Y. Fang, Y. Lv, F. Gong, Z. Wu, X. Li, H. Zhu, L. Zhou, C. Yao, F. Zhang, G. Zheng, D. Zhao, *J. Am. Chem. Soc.* **2015**, 137, 2808; n) H. Zhang, O. Noonan, X. Huang, Y. Yang, C. Xu, L. Zhou, C. Yu, *ACS Nano* **2016**, 10, 4579; o) F. Xu, Z. Tang, S. Huang, L. Chen, Y. Liang, W. Mai, H. Zhong, R. Fu, D. Wu, *Nat. Commun.* **2015**, 6, 7221; p) Y.-X. Wang, J. Yang, S.-L. Chou, H. K. Liu, W.-x. Zhang, D. Zhao, S. X. Dou, *Nat. Commun.* **2015**, 6, 8689; q) T. Yang, H. Ling, J.-F. Lamonier, M. Jaroniec, J. Huang, M. J. Monteiro, J. Liu, *NPG Asia Mater.* **2016**, 8, e240; r) J. Liu, N. P. Wickramaratne, S. Z. Qiao, M. Jaroniec, *Nat. Mater.* **2015**, 14, 763.
- [11] a) J. Hou, T. Cao, F. Idrees, C. Cao, *Nanoscale* **2016**, 8, 451; b) S. Zou, X. Xu, Y. Zhu,

- C. Cao, *Microporous and Mesoporous Mater.* **2017**, 251, 114.
- [12] C. Bernal, M. Mesa, M. Jaber, J. L. Guth, L. Sierra, *Microporous Mesoporous Mater.* **2012**, 153, 217.
- [13] R. Xing, N. Liu, Y. Liu, H. Wu, Y. Jiang, L. Chen, M. He, P. Wu, *Adv. Funct. Mater.* **2007**, 17, 2455.
- [14] a) J. G. Croissant, Y. Fatieiev, N. M. Khashab, *Adv. Mater.* **2017**, 29, 1604634; b) L. Zhou, Z. Zhuang, H. Zhao, M. Lin, D. Zhao, L. Mai, *Adv. Mater.* **2017**, 1602914; c) C. Chen, H. Wang, C. Han, J. Deng, J. Wang, M. Li, M. Tang, H. Jin, Y. Wang, *J. Am. Chem. Soc.* **2017**, 139, 2657; d) X. Du, S. Z. Qiao, *Small* **2015**, 11, 392.
- [15] Q. Huo, D. I. Margolese, U. Ciesla, P. Feng, T. E. Gier, P. Sieger, R. Leon, P. M. Petroff, F. Schuth, G. D. Stucky, *Nature* **1994**, 368, 317.
- [16] G. M. Whitesides, B. Grzybowski, *Science* **2002**, 295, 2418.
- [17] a) S. Jun, S. H. Joo, R. Ryoo, M. Kruk, M. Jaroniec, Z. Liu, T. Ohsuna, O. Terasaki, *J. Am. Chem. Soc.* **2000**, 122, 10712; b) S. Inagaki, Y. Fukushima, K. Kuroda, *J. Am. Chem. Soc., Chem. Commun.* **1993**, 680; c) G. S. Attard, J. C. Glyde, C. G. Goltner, *Nature* **1995**, 378, 366.

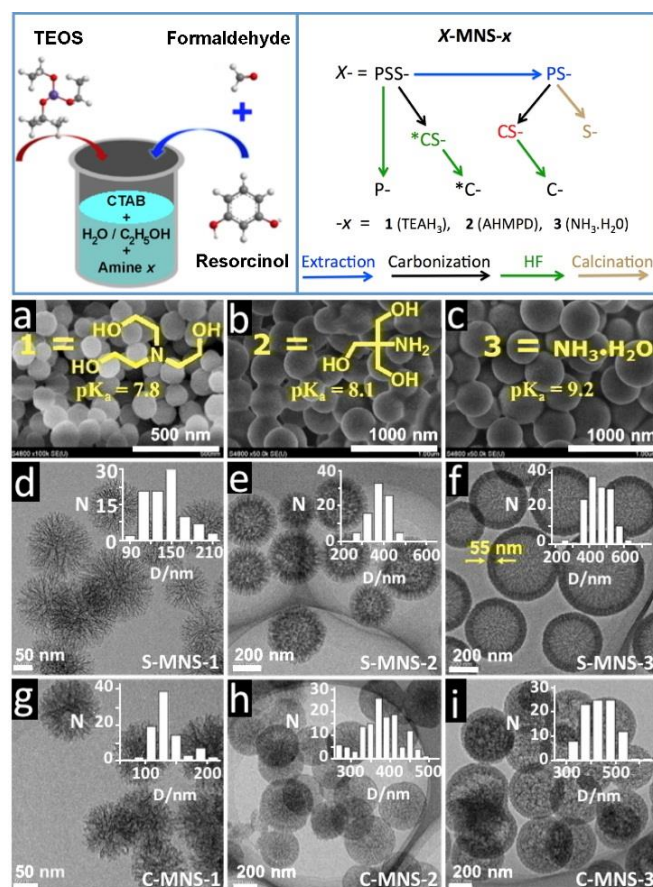


Figure 1. Reaction scheme, synoptic of sample nomenclature, SEM and TEM images. Scheme (top left), nomenclature (top right) SEM images of the carbonized hybrid nanospheres CS-MNS-x (a to c), direct TEM images of yin and yang single phases C- or S-MNS-x (d-i) with insets for particle size distribution (PSD).

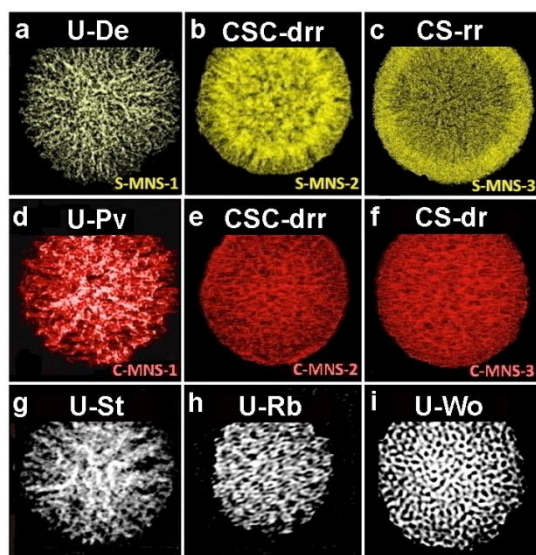


Figure 2. Inverted contrast TEM images of nanospheres adopting different topologies and pore arrays: (a to f) C- or S-MNS-x samples and (g to i) S-MNS from ref.3; nomenclature provided in Table 1 and explained in SI.

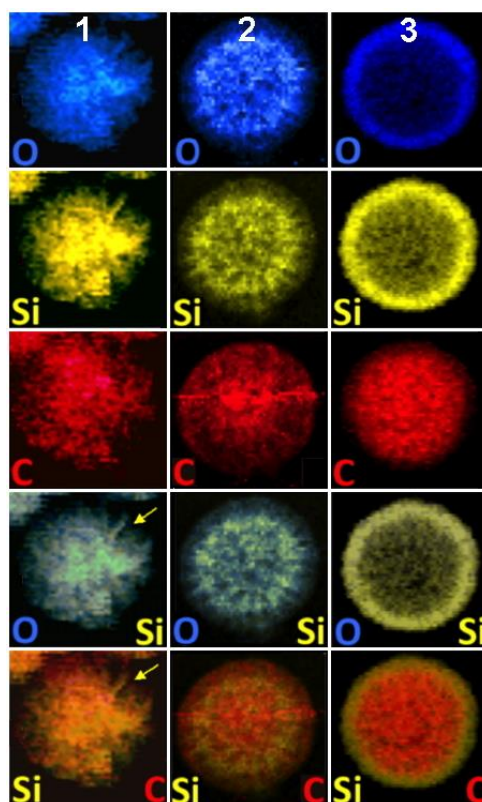


Figure 3. EDX elemental analysis. Mappings of O (blue), Si (yellow) and C (red) of CS-MNS-x yin and yang hybrids ($x = 1, 2$ and 3 for left, middle and right column, respectively); yellow arrows pointing a location where the carbon nanophase wraps up a silica dendrite; Rows 4 and 5, superposition of O + Si and Si + C mappings.

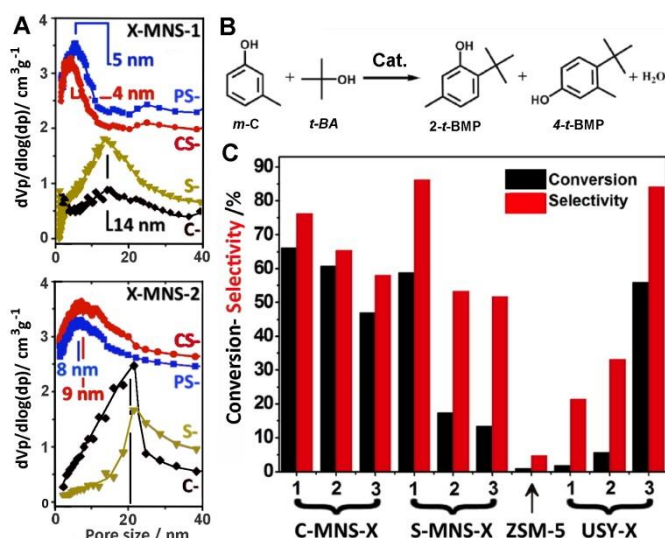


Figure 4. Pore size distribution (PSD), Reaction scheme and Catalytic activity. (A) X-MNS-1 and b) X-MNS-2 (BJH model), B top) reaction scheme of *m*-cresol (*m*-C) with *tert*-butyl-alcohol (*t*-BA) converted into 2-*tert*-butyl-5-methylphenol (2-*t*-BMP) or 4-*tert*-butyl-5-methylphenol (4-*t*-BMP), B bottom) catalytic conversion (black bar) and selectivity (red bar) of various silica and carbon nanospheres after functionalization by sulfonic acid groups including zeolites ZSM-5, USY-1, dealuminated USY-2 and USY-3 and C) specific micelle templated distance between nanophases (color code in Fig. 5).

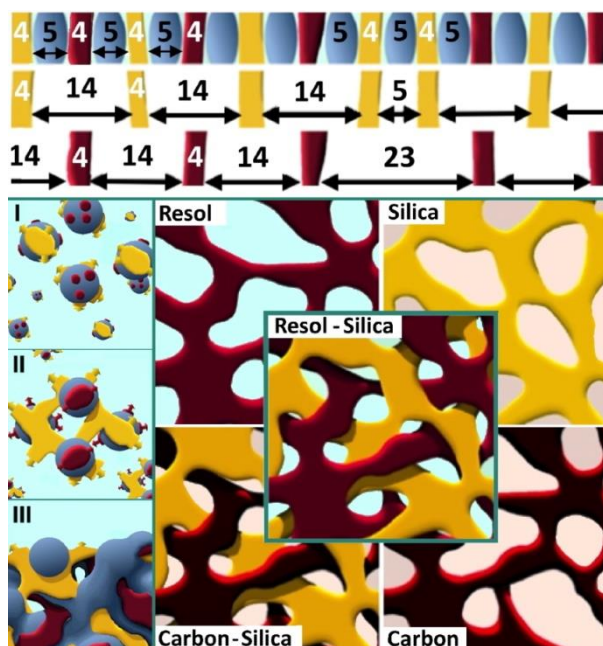


Figure 5. Key mechanism steps, specific spacings and derivatized nanophases: (left column) main steps of syntactic phase entanglement, and (right set of five windows) derivatized syntactic nanophases; micelles (blue), silica phase (yellow), polymer (purple-red) and carbon (black) phases.

Table 1. Morphology descriptors for topology and pore array.

Topology	Code	Pore array	Code
Uniform	U	disordered	d
core-shell	CS	center radial	r
core-shell-corona	CSC	dendritic	De
hollow ^a	Hw	stellar	St
-	-	raspberry	Rb

^a)described in the triphasic resol-surfactant-silica system by other groups in refs. 7a and 11.

Table 2. Textural and structural characteristics of X-MNS-x nanospheres.

Sample ^{a)}	S _{BET} ^{b)} (m ² /g)	V _{total} ^{c)} (ml/g)	D _{BJH} ^{d)} (nm)	PSD ^{e)} (nm)	Morphology: topology & pore array ^{f)}
PS-MSNS-1	495	0.57	5 (2-10)	-	U-Pv/De
CS-MSNS-1	321	0.37	4 (2-8)	-	U-Pv/De
*CS-MSNS-1	221	0.56	12 (6-25)	-	U-Pv/De
S-MSNS-1	577	1.65	14 (8-20)	140 ± 20	U-De
C-MSNS-1	806	1.46	14 (8-20)	135 ± 15	U-Pv
PS-MSNS-2	83	0.12	9 (5-20)	-	CSC-drr/drr
CS-MSNS-2	374	0.31	9 (5-20)	-	CSC-drr/drr
*CS-MSNS-2	291	0.35	14 (9-30)	-	CSC-drr/drr
S-MSNS-2	340	1.11	23 (15-40)	380 ± 25	CSC-drr
C-MSNS-2	747	1.61	19 (9-25)	375 ± 30	CSC-drr
PS-MSNS-3	68	0.07	6 (2-10) & ~ 26	-	CS-dr/rr
CS-MSNS-3	449	0.32	3 (2-7) & ~ 26	-	CS-dr/rr
*CS-MSNS-3	368	0.44	24 (12-35)	-	CS-dr/rr
S-MSNS-3	513	0.70	10 (6-16) & ~ 42	480 ± 40	CS-rr
C-MSNS-3	739	1.51	9 (5-13) & 22	440 ± 38	CS-dr

a) P, C, S phases, = Polymer, Carbon, Silica and, $x = 1-3$, **1** = TEAH₃, **2** = AHMPD and **3** = NH₃·H₂O, respectively, *C for carbonization in the presence of the surfactant; **b)** specific surface area measured from N₂ physisorption isotherm (Fig. S6), and surface per volume unity in m²/cm³ or volumetric surface area calculated from bulk densities of amorphous silica and resol-formaldehyde of 2.3 and 1.25 g/cm³, respectively; **c)** total pore volume measured at P/Po = 0.99; **d)** pore diameter calculated at the maximum of the distribution using the adsorption branch and the BJH theoretical model, in parenthesis range of the distribution estimated from half height of the distribution and, secondary pore size distribution indicated after the symbol “~” when detected; **e)** particle size distribution (PSD) from TEM; **f)** when both *yin* and *yang* nanophases are still entangled, the pore array is indicated in the order of the phases given in the sample name (here P or C provided before S).